Article

Not peer-reviewed version

Flood Extent Delineation and Exposure Assessment in Senegal Using Google Earth Engine: The 2022 Event

Bocar SY *, Fatoumata Bintou BAH , Hy Dao

Posted Date: 25 April 2024

doi: 10.20944/preprints202404.1552.v1

Keywords: flood extent mapping; flood exposition assessment; remote sensing; Google Earth Engine; Sentinel-1; hydrological and hydraulic modelling

 doi:10.20944/preprints202404.1552.v1

Article

Flood Extent Delineation and Exposure Assessment in Senegal using Google Earth Engine: the 2022 event

Bocar SY [1,*], Fatoumata Bintou BAH [1] and Hy Dao [2,3]

[1] Laboratory of Applied Geomatic (LAG), Department of Geoscience and Environment, Université Amadou Mahtar Mbow, Rue 21*20, 2ème arrondissement, pole urbain de Diamniadio, Sénégal
[2] Department of Geography and Environment, Geneva School of Social Sciences, University of Geneva, 66 Boulevard Carl-Vogt, Geneva, 1205, Switzerland
[3] Institute for Environmental Sciences, University of Geneva, Boulevard Carl-Vogt 66, Geneva, 1205, Switzerland
* Correspondence: bocar.sy@uam.edu.sn

Abstract: This study addresses the pressing need for flood extent and exposure information in data-scarce and vulnerable regions, with a specific focus on West Africa, particularly Senegal. Leveraging the Google Earth Engine (GEE) platform and integrating data from Sentinel-1 SAR, Global Surface Water, HydroSHEDS, Global Human Layer Settlement, and MODIS Land Cover, our primary objective is to delineate flood extents and compare them with centennial flood-prone areas, offering a comprehensive assessment of exposure during the period from July to October 2022 across Senegal's 14 regions. The findings underscore a total inundation area of 2 951 square kilometers, impacting 297 142 people, 175 square kilometers of urban and 16 square kilometers of crops. Notably, August witnessed the largest flooded areas, reaching 780 square kilometers, constituting 0.40% of the country's surface. Subsequent regions, including Saint-Louis, Ziguinchor, Fatick, and Matam, experienced varying extents of flooding, with August data showing a 1.34% overall overlap compared to centennial flood-prone areas derived from hydrological and hydraulic modeling. This low percentage reveals the distinct purposes and natures of the two approaches (remote sensing and modeling), as well as their complementarity.Turning to flood exposure, August emerges as the most critical month, affecting 76 595 people (0.43% of the total population). Dakar, Diourbel, Thiès, and Saint-Louis regions bore substantial impacts, affecting 100 707, 57 648, 31 579, and 26 581 people, respectively. These findings emphasize the imperative for comprehensive disaster preparedness and mitigation efforts. The study provides a crucial national-scale perspective to guide Senegal's authorities in formulating effective flood management, intervention, and adaptation strategies.

Keywords: flood extent mapping; flood exposition assessment; remote sensing; Google Earth Engine; Sentinel-1; hydrological and hydraulic modelling

1. Introduction

The anticipated impacts of climate change are set to exacerbate the frequency and severity of hydro-climatic extreme events, with a particular focus on floods and droughts in vulnerable regions like numerous African countries[1] Among these events, floods stand out as notably prevalent and consequential in Africa[2]. Over the past two decades (2002-2022), floods have accounted for 64% of all disasters on the continent. During this period, Africa endured 793 flood disasters, resulting in over 16 900 fatalities, and adversely affecting the lives of 58 million people [3]

Within West Africa, Senegal has borne period burden of flooding, witnessing 13 flood events over the same period, and impacting a substantial 23 874 963 individuals [3]. The consequences extend beyond the loss of human lives to include the destruction of farmlands. Notably, the troubling trend of entire regions facing inundation on a biennial basis is on the ascent. This rise can be attributed to the confluence of factors such as climate change, persistent poverty, and rapid urbanization [4,5].

The compounding effects of continuous socio-economic changes, including rapid urbanization and agricultural expansion [6,7] further elevate the vulnerability to flooding. These changes

 doi:10.20944/preprints202404.1552.v1

contribute significantly to the escalating flood risk, as evidenced by research by Hirabayashi [8]. In essence, the convergence of climate change and anthropogenic factors amplifies the challenges faced by regions like Senegal, necessitating a comprehensive understanding and effective mitigation strategies to safeguard both lives and livelihoods.

Despite the concerted efforts by Senegalese authorities, involving the construction of retention basins, pipelines, pumping stations, and even the relocation of residents, the measures have been implemented, but their impact has not been sufficient[9,10]. One contributing factor to this limitation is the absence of a comprehensive and complete mapping of flooded areas and flood exposure. Such mapping is crucial for precisely targeting spatially effective mitigation strategies, as emphasized by Li et al [11], providing invaluable insights for government and disaster relief agencies.

The lack of comprehensive flooded area mapping prevents the visualization of regions susceptible to specific flood scenarios, as highlighted by Sy et al. [12]. Additionally, the absence of detailed flood exposure mapping hampers the assessment of the population and assets situated within these vulnerable areas, a critical aspect emphasized by Muis et al [13]. The inadequacy in mapping these aspects undermines the ability of authorities to implement targeted and efficient mitigation measures, hindering the overall effectiveness of flood risk reduction initiatives. Addressing these gaps in mapping is paramount for enhancing the resilience of Senegal and ensuring that mitigation efforts align with the specific needs of the exposed population and vulnerable areas.

Significant progress has been made in mapping floods and assessing exposure at both local and national scales notably with the development of Earth Observation Systems equipped with increased revisit frequency and higher spatial resolution, along with easy access to both satellite imagery and data from other sources [14-11]. Google Earth Engine (GEE), launched in 2010, has evolved into one of the world's most extensive publiclyy accessible Earth observation catalogs, amalgamating data from satellites and other sources. GEE functions as a geospatial data and image visualization and processing tool, providing access to a plethora of international and regional datasets. This data is complemented by cloud computing resources, facilitating the extraction of timely, precise, and high-resolution information about the Earth's surface condition. GEE boasts a vast geospatial data repository, encompassing regularly updated Sentinel-1 GRD ("Ground Range Detected") data [14]. The Synthetic Aperture Radar (SAR) capability of Sentinel-1 makes it particularly valuable for flood extent mapping, as it offers frequent observations even in adverse weather conditions [15]. Flooded areas appear dark in SAR images due to their low backscatter signal, enabling differentiation from other land cover categories like agricultural and built-up areas [16] . The availability of analysis-ready SAR datasets on GEE is a significant advancement in remote sensing applications. GEE's dataset encompasses more than four decades of archived earth observation imagery, including SAR data [17], facilitating the continuous monitoring of global water bodies and their dynamics, including flood mapping [11]. Many studies have used SAR images in Google Earth Engine to map flood areas [16–21]. Even though some studies focus on flood exposure globally [11–22], until now, it has received little attention in data scarce and developing country [23–25]. These scarce flood exposure assessment studies primarily evaluate land cover classes such as "urban areas" or solely rely on population mapping layers.

Our study contributes value by comparing the largest flooded areas obtained from Google Earth Engine (GEE) with centennial flood-prone areas derived from hydrological and hydraulic models. Remote sensing data from GEE can provide real-time information on flooded areas, while hydrological and hydraulic models simulate potential flood scenarios. Identifying discrepancies between remote sensing data and model outputs highlights areas of uncertainty or limitations in either approach. Analyzing these differences helps identify potential reasons for discrepancies, such as inaccuracies in the models, limitations of remote sensing techniques, or variations in data resolution. By comparing outputs from remote sensing data with those from hydrological and hydraulic models, we validate the relevance of both approaches. A close match between the two datasets increases confidence in the reliability of the models and remote sensing techniques used. Understanding how remote sensing data and modeling outputs align or differ enables decision-makers to better prioritize areas for flood management interventions. This comparison informs the

 doi:10.20944/preprints202404.1552.v1

development of more effective strategies for flood mitigation, early warning systems, and emergency response planning. Overall, comparing remote sensing data with hydrological/hydraulic models enhances our understanding of flood dynamic and improves flood risk management in the study area by leveraging the strengths of both approaches.

While, prior studies in Senegal have investigated spatiotemporal solutions using remote sensing, citizen science, and multi-criteria modeling at the local scale [12–26], there is a lack of such research on a national scale. To address this gap, the Senegalese government, through the PGIIS project ("Projet de Gestion Integrée des Inondations au Sénégal"), has recently initiated a geographic information system for mapping flood-prone areas and conducting flood hazard assessments at a national level using hydraulic and hydrological modeling [28]. It is notable that none of the studies in flood use GEE. Furthermore, there is a notable absence of spatiotemporal studies on exposure assessment.

In contrast to local-scale studies and recent national-scale initiatives, this study adopts a spatial-context approach utilizing Sentinel-1 images and relevant data on population distribution, density, and land cover from GEE. The objective is to map flooded areas including their comparison with centennial flood prone areas from PGIIS and assess flood exposure in terms of population, urban and farmland across Senegal's 14 regions for the 2022 event. Our choice has focused on the floods of 2022, considering that Senegal experienced above-average precipitation and an unusually high total precipitation[29], as well as very intense flooding throughout the country[30,31].

This study seeks to: (1) employ a spatial-context method to map flooded areas for the four months of the 2022 event on a national scale using the GEE tool, (2) compare the most flooded areas month with the 100-year flood-prone areas derived from hydrological and hydraulic modeling, evaluating the accuracy of flood detection - enabling the prioritization of mitigation measures by region, and (3) evaluate exposure in terms of population, urban and cropland for the four months of the 2022 flood event.

2. Study Area

The Google Earth Engine approach was applied to all 14 regions of Senegal in West Africa (Figure 1). Situated between 12°8 and 16°41 north latitude and 11°21 and 17°32 west longitude, Senegal shares borders with Mauritania to the north, Mali to the east, Guinea Bissau and Guinea Conakry to the south, and the Atlantic Ocean to the west, boasting a coastline spanning 700 km. Encompassing an area of 196 722 km2 [32], Senegal is home to approximately 18 million inhabitants as of 2023, with a population density of around 92 inhabitants per km2 [33]. The terrain is predominantly flat, with nearly 75% of the landmass lying at an elevation of less than 50 m. The highest point, reaching 581 m above sea level, is situated in the southeastern foothills of the Fouta-Djalon Mountain [28].

Senegal is administratively divided into 14 major regions (decree no. 2013-10, Republic of Senegal).

Preprints.org (www.preprints.org) | NOT PEER-REVIEWED | Posted: 25 April 2024 doi:10.20944/preprints202404.1552.v1

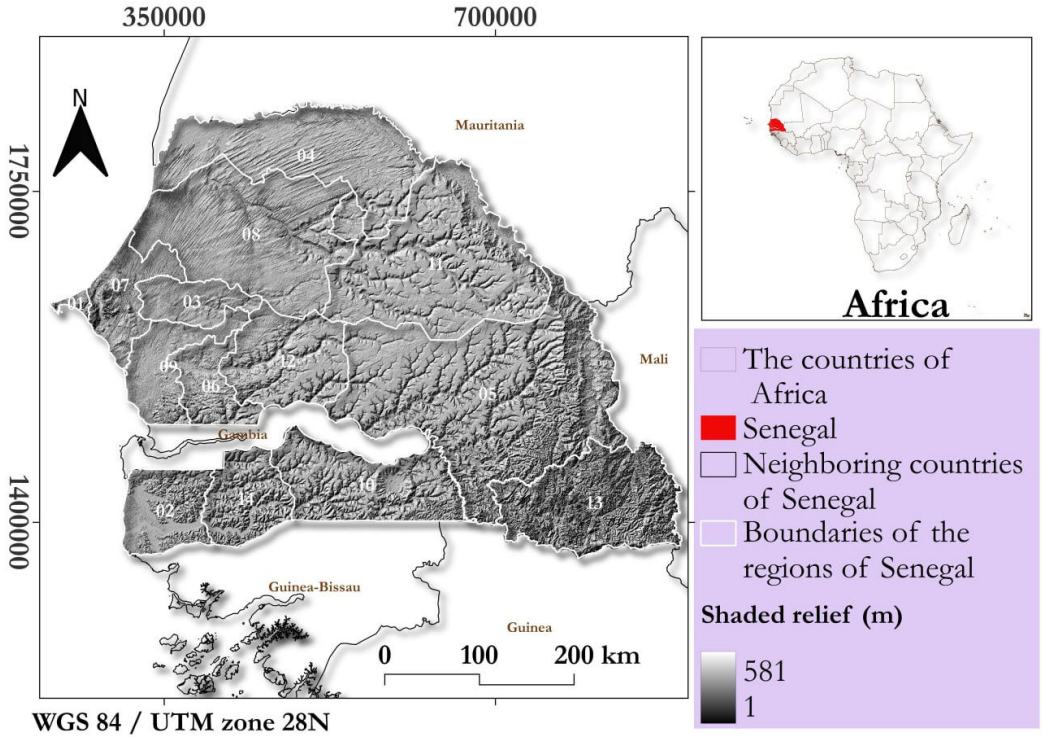

Figure 1. Location of the study area. The insert in the right corner locates our study area on the continent of Africa with bordering countries. The central map represents our study area Senegal with 14 regions, with shaded relief as the map background. The 14 regions are designated by numbers from 1 to 14. The corresponding names are provided in Supplement Table S1.

Senegal features a diverse range of landscapes encompassing both urban and rural regions. Urban centers such as Dakar, Thiès, Kaolack, and Saint-Louis play crucial roles in economic, cultural, and political spheres, with some urban regions containing rural areas as well. Similarly, certain rural regions like Ziguinchor, Fatick, Diourbel, Louga, Kolda, Matam, Tambacounda, Kédougou, Kaffrine, and Sédhiou also include urban parts, albeit less developed. These cities and regions are characterized by bustling markets, modern infrastructure, and vibrant cultural scenes, or by agricultural and fishing activities in rural zones[34].

Senegal's climatic regime is characterized by two main seasons:

- The dry season (November to April-May) is marked by the prevalence of maritime trade winds towards the west and continental trade winds inland.
- The rainy season (May-June to October) is dominated by the monsoon flow from the St. Helena anticyclone.

The regions in Senegal have experienced significant and recurring flooding, resulting from various phenomena: overflow flooding of perennial rivers, overflow flooding of temporary watercourses, urban runoff, rural runoff, flooding due to stagnation in depressions or endoreic zones, flooding due to rising groundwater. In some cases, these various phenomena combine to exacerbate their consequences.

3. Materials and Methods

3.1. Data

In this study, we utilized GEE for all satellite data processing. The comparison of flooded areas with flood prone areas were processed using ArcGIS Pro, including the final maps processing and symbology. Additionally, Excel was employed for tabular data storage and histogram production. The selection of the GEE platform for this research was motivated by its unique capabilities, allowing

 doi:10.20944/preprints202404.1552.v1

for the direct utilization of the GEE database and providing access to an extensive catalog of satellite images, as well as a wide array of geospatial datasets (https://earthengine.google.com). GEE boasts a public data archive containing over 40 years' worth of global imagery (https://earthengine.google.com). As outlined in Table 1, all data layers were accessed from GEE data catalog and processed within the GEE cloud-computing platform[17]. Only administrative boundaries of Senegal country and areas prone to 100-year floods were obtained from other sources. All raster and vector layers were saved in Senegal's coordinate system, specifically, UTM-28N (EPSG: 32 628).

Table 1. Overview of data layers used for flooded areas including comparison of flooded areas and flood prone areas 100 years and flood exposure.

Layers names	Sources	Date	Type	Resolution (m)
Administrative limits	LGA*	2020	Vector	
Sentinel-1 images	Copernicus	**	Raster	10
		***		
Flood prone areas 100 Years	PGIIS	2023	Raster	
Global Surface Water	EC / JRC	01-01-2022	Raster	30
HydroSHEDS	WWF US	22-02-2020	Raster	30
Global Human Settlement Layer	EC / JRC	31-12-2015	Raster	250
MODIS Land Cover	NASA	01-01-2020	Raster	500

* Laboratory of Applied Geomatic (Amadou Mahtar Mbow University) ;**before flooding: 2022-03-02 to 2022; ***after flooding: 2022-20-07 to 31-07-2022; 01-08-2022 to 31-08-2022; 01-10-2022 to 10-10-2022

The methodology employed in this study heavily inspires to the recommended guideline set forth by the United Nations' recommended guidelines for flood mapping and exposure assessment using SAR Sentinel-1 data within the Google Earth platform.

(https://www.un-spider.org/advisory-support/recommended-practices/recommended-practice-google-earth-engine-flood-mapping/step-by-step).

To begin, we conducted monthly flood mapping using remote sensing techniques at a spatial scale of 10 meters during wet season (July to October). This was achieved by utilizing Sentinel-1 radar data available from 2022 (2022-20-07 to 31-07-2022; 01-08-2022 to 31-08-2022; 01-10-2022 to 10-10-2022), the Global Surface Water (GSW) layer to identify surface water distribution from 1984 to 2022, and a HydroSHEDS from 2020. Next, we compared the flood extents observed through remote sensing with 100-year flood prone-areas, which were determined through hydrological and hydraulic modelling provided by the PGIIS in ArcGIS Pro. Finally, we assessed flood exposure by integrating the flooded areas with MODIS land cover data and layers depicting the distribution and population density, which were obtained from Global Human Settlement Layer in Google Earth Engin (Figure 2).

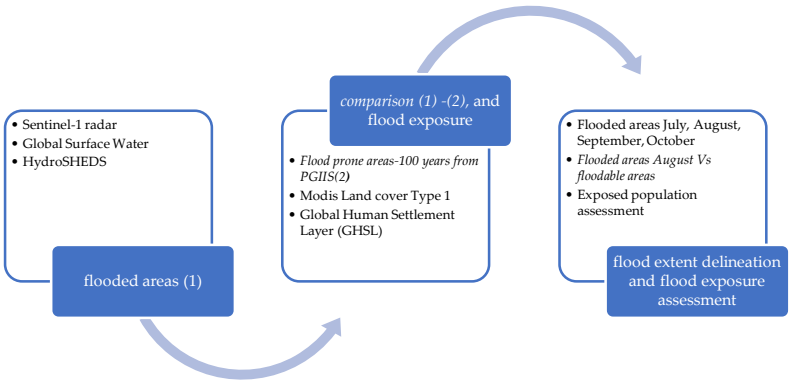

 doi:10.20944/preprints202404.1552.v1

Figure 2. Framework for flood extent delineation (1), and flood exposure assessment, with comparison of flood extent by remote sensing in Google Earth Engine (1) versus hydrological and hydraulic modelling from PGIIS (2). The process of this comparison is to be read in this figure using italicized text. The code is available.

https://code.earthengine.google.com/7563c82272972ebd9c7130257d0d5483

3.2. Mapping the Spatial and Temporal Distribution of Flooded Areas

To obtain information of flooded areas using Sentinel-1 on Google Earth Engine, we followed a four-step process.

Step 1: Specification of the location of our study area

This initial step involved defining geographical boundaries of our study area. This information served to constrain the processing area, thus preventing unnecessary computations. To delineate the spatial processing extent, we utilized a Shapefile (.shp) depicting the administrative limits of Senegal, encompassing all 14 regions. This administrative boundary layer for Senegal was extracted from Laboratory of Applied Geomatic of Amadou Mahtar Mbow University.

Step 2: Time frame and sensor parameters

In addition to defining the area of interest, we specified the pre-flood and post-flood periods for each month of flooding (July, August, September, and October), as outlined in Table 1. By defining periods, rather than individual dates, we ensured coverage of the entire Senegal region by selecting enough tiles. We used Sentinel-1 Synthetic Aperture Radar (SAR) C- band (5.4 GHz) data provided by the European Space Agency [35]. These images are acquired at intervals of at least every 12 or 6 days for each point on the globe depending on the availability of Sentinel-1 imagery [36]. With a spatial resolution of 10 meters, we accessed and clipped the level-1 Ground Range Detected (GRD) processed product in GEE for the study area during the pre-flood and post-flood period (see the footer of Table 1). Furthermore, for our analysis, we chose 'VH' polarization over 'VV' polarization. VH' polarization is widely recommended for flood mapping [16–37] because it is more sensitive to changes at the ground surface, while 'VV' polarization is more sensitive to vertical structures and can be useful for delineating open water from the ground surface (e.g., detecting the coastline or a large expanse of water that has appeared after a flood).

We selected the ascending passage direction, which is consistent with our Senegal study area. In the world, some areas are covered only by descending or only ascending passage directions, while others are covered by both directions [39]. When detecting changes, it is necessary to select the same passage direction for the images being compared to avoid false positive signals caused by differences in viewing angle.

Step 3: Mosaicking images and applying the speckle filter.

This step involves sharpening the images before and during the flooding period, for example, by removing thermal noise and performing a radiometric correction. We applied a 3*3-pixel median filter to remove speckle effects in SAR images, resulting in smoother images [38–40].

Step 4: Generation of flooded areas maps

This step is divided into two parts. In the first part, we aimed to detect changes between the pre- and post-flooding layers to create a difference layer on which thresholding is applied (threshold of 1.25; pixel above 1.25 assigned a value of 1; pixel below 1.25 assigned a value of 0 [38–40]. The resulting binary raster layer represents the potential flooded areas. In the second part, we intersected the generated binary layer with the Global Surface Water (GSW) layer to exclude permanent water (water present for more than 10 months, e.g., Lakes). This dataset with a 30-meter resolution has been extracted from EC/JRC. It contains maps of the location and temporal distribution of surface waters from 1984 to 2018 and provides statistics on the extent and evolution of these water surfaces across the globe. It was clipped to our study area. Finally, we used the Digital Elevation Model layer to remove areas with a slope greater than 5%, as these areas are rarely flooded [12]. This raster layer was obtained from the Shuttle Radar Topography Mission on HydroSHEDS which offers suite of

 doi:10.20944/preprints202404.1552.v1

georeferenced raster in tiles at a resolution of 30 meters and mosaicked to cover the entire country. The resulting layer represents the flooded areas.

3.3. Comparison of Existing 100-Years Flood Prone Areas with Flooded Areas Mapping Using Sentinel-1, GSW Layers and Digital Elevation Model

The 100-year flood-prone areas were obtained from the results of hydraulic and hydrological modelling. This modelling was commissioned by the Senegalese Government through PGIIS with the aim to providing flood management solutions at a national scale. We compared this layer with our Sentinel-1 derived flood areas using GEE platform. This comparison had two primary objectives: first, to evaluate the accuracy of flood detection in Senegal, enabling the prioritization of mitigation measures by region. This comparison was carried out using the spatial join and zonal statistique tools of ArcGIS Pro between the boundary layers of the regions, the flooded areas obtained from GEE, and the flood-prone areas from the centenal model derived from the PGIIS hydrological model.

3.4. Estimation of Flood Exposure

3.4.1. Exposed People

To estimate flood exposure across Senegal's 14 regions, in GEE, we utilized the Global Human Settlement Layer from the European Commission's Joint Research Center (EC / JRC) [41]. This layer with a resolution of 250 meters and was last updated in 2015, provides information on the population count per cell . Since our analysis was conducted at a 30-meter resolution, we resampled this raster layer to match using nearest neighboor interpolation. To avoid multiple counting of population for the approximately 8 x 8 x 30 m cells within the 250m cells when using nearest neighbors, the approach is to allocate the 250m population to 30m.cells using HydroSHEDS data. This ensures that each person is counted only once, regardless of how many smaller cells they may overlap within the larger 250m cells. This method helps to maintain the accuracy of population counts and avoids overestimation due to double-counting.

To integrate the flood extent layers for the months of July, August, September, and October with the population data, we first reprojected the flood area rasters to align with the resolution and projection of the population dataset. Next, we conducted a spatial intersection between each flood extent layer and the population dataset, resulting in the creation of new raster layers. Finally, to calculate the total number of individuals exposed to flooding, we summed the pixel values within the exposed population raster.

3.4.2. Affected Cropland and Urban

To estimate the extent of affected cropland, we utilized the MODIS Land Cover Type product, which offers a spatial resolution of 500 meters and is updated annually. Given that our analyses were conducted at a 30-meter resolution, we resampled the land cover raster to match using nearest neighbor interpolation. This dataset is currently the only global dataset on Land Cover available in the Google Earth Engine (GEE) data catalog. Within the Land Cover Type 1 band, there are 17 classes, including two relevant cropland classes: class 12, indicating areas with at least 60% cultivation, and class 14, representing cropland/natural vegetation mosaics where small-scale cultivation occupies 40-60% of the area alongside natural tree, shrub, or herbaceous vegetation.

To identify affected cropland, we extracted these cropland classes from the MODIS dataset and intersected them with the flooded areas in July, August, September, and October, which were resampled to match the scale and projection of the MODIS layer. Similarly, we calculated the areas of affected urban and rural regions using the same methodology applied to the flooded areas.

To identify affected urban areas, we extracted the 'Urban Class 13' from the 'Land Cover Type 1' band of the MODIS dataset. It's worth noting that in this process, the estimation of affected urban areas may be conservative due to challenges in detecting water within built-up areas, potentially leading to underestimation.

 doi:10.20944/preprints202404.1552.v1

4. Results

4.1. Mapping of flooded Areas Using Sentinel-1, GSW Layers and Digital Elevation Model

We obtained floods extents for the months of July, August September, and October in Senegal, using Sentinel-1images on GEE platform. The methodology is described in Figure 2. We determined a total inundation area of 2 951 square kilometers. It is noteworthy that during this event, all regions of the country experienced flooding at least once (Figure 3, Supplement Material S2).

Further analysis indicates that August witnessed the most widespread flooding, covering 779.54 square kilometers or 0.40% of the country's total surface area. September and July followed closely with respectively 746.80 square kilometers and 723.98 square kilometers or 0.38% and 0.37%, while September experienced the smallest extent of flooding encompassing 700.68 square kilometers or 0.36% (Figure 3, Supplement Material S2).

A closer look at the regions flooded shows that the Saint-Louis, Ziguinchor, Matam and Fatick regions recorded the most extensive flooding (Figure 3, Supplement Material S2) with a mean area of 253.06 square kilometers, 93.55 square kilometers, 74.24 square kilometers, 86 square kilometers and 70.75 square kilometers respectively. These areas correspond approximately 1.31%, 1.27% ,0.25% and 1.03 of the total land area of these regions.

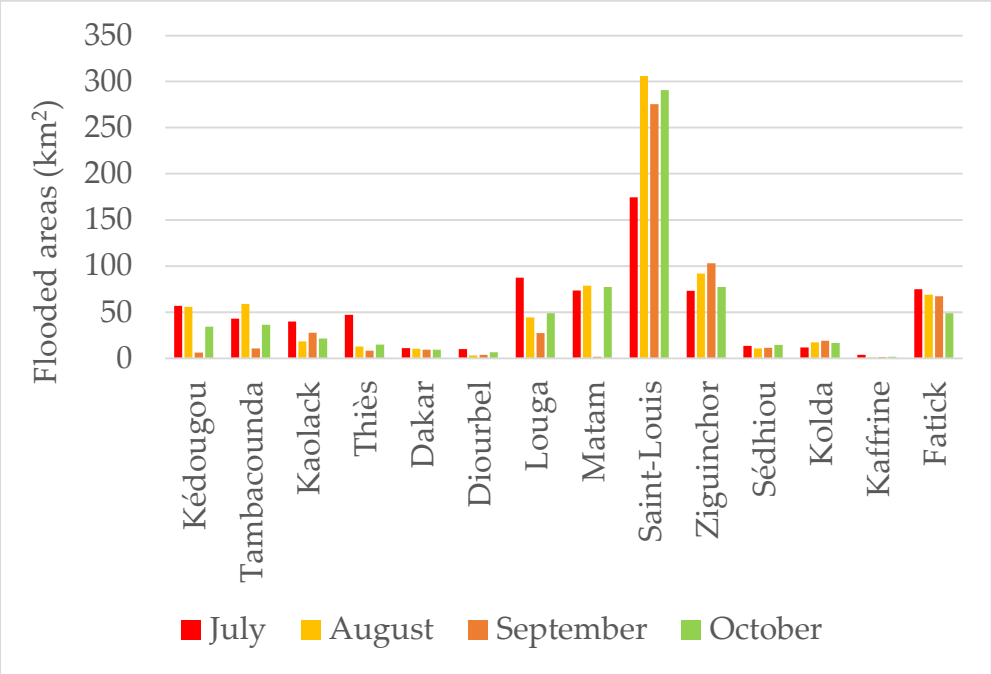

Figure 3. Histogram of flooded areas based on Sentinel-1, GSW and HydroSHEDS in 2002 events per region and months, July (red), August (yellow), September (orange) and October (light green).

In terms of mapping, slight differences appear between the spatial location of the flooded areas for the months of July, August, September, and October, showcasing variations of 8%. The GEE shows that in the Saint-Louis region the main flooded areas were in the North-West, North-East, and North part of the region, but some flooded areas occur in the central part and in the South-East (Figure 4). In the Ziguinchor region, the main flooded areas are in the central and upper parts in low-lying areas, but some residual flooded areas are also found in the northwest and southeast (Figure 4).

 doi:10.20944/preprints202404.1552.v1

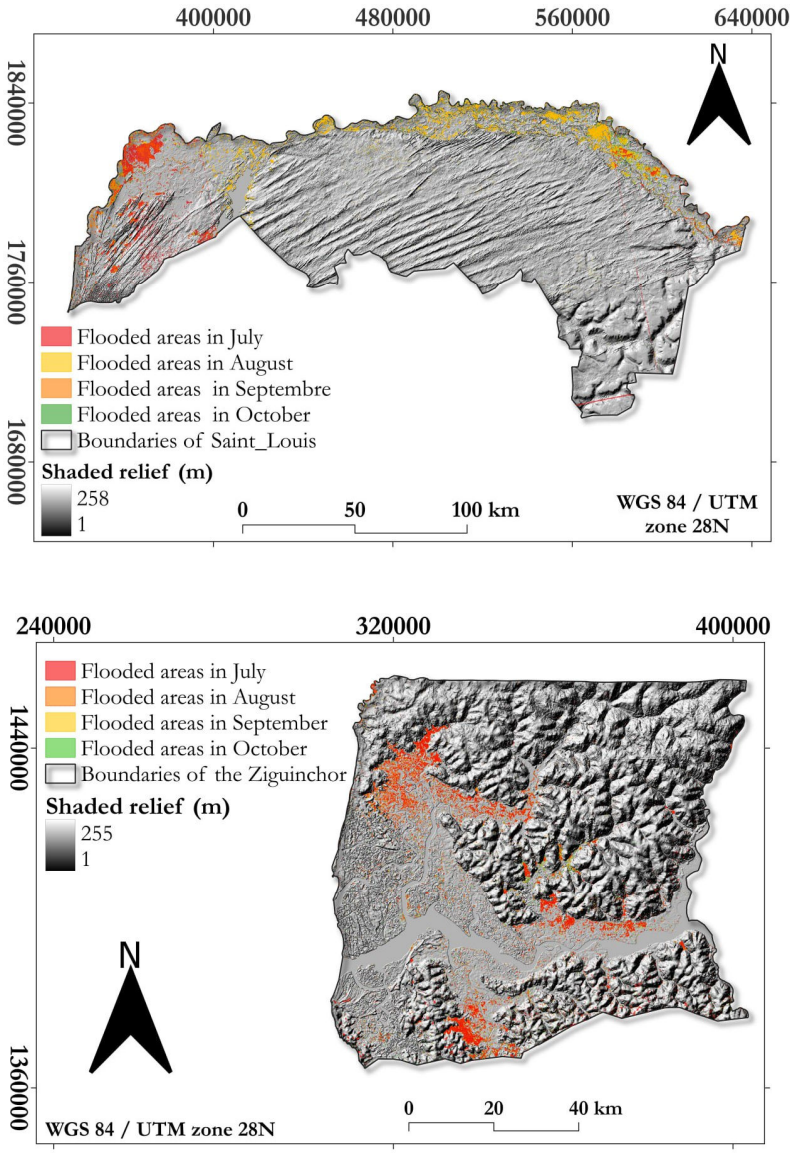

Figure 4. Spatial distribution of flooded areas based on Sentinel-1, GSW and HydroSHEDS in 2002 events in the 2 most flooded regions (Saint-Louis and Ziguinchor).

4.2. Comparison Flooded Areas Obtained by Remote Sensing (Google Earth Engine) with 100-year Flood Prone Areas Obtained Using Hydrological And Hydraulic Modelling

Flood extents for the 2022 events were obtained from the GEE methodology described in figure 2 and then compared to the results derived from the PGIIS that have modelled 100-year flood prone areas to measure the extent of this event. Data obtained through the Google Earth approach revealed that the month of August was the most widespread, whereas the month of September event was the smallest (Figure 3). The data obtained in August through the GEE approach has been compared with hydrological and hydraulic modelling from PGIIS. The flooded areas in August provided by GEE for the 2022 event are smaller than those indicated by the modeling of 100-year floods (Table 2), showing a total overlap of 1.43% across all 14 regions of the country, ranging from 0.04% in the Kaffrine region to 10.19% in the Dakar region. (Table 2).

 doi:10.20944/preprints202404.1552.v1

Table 2. Flooded areas obtained Google Earth Engine (remote sensing) in August in the second column and floodable areas from PGIIS (hydrological and hydraulic modelling) in third column with the percentage of overlapping areas between remote sensing and hydrological modelling in fourth column.

Region of Senegal	Flooded areas August from remote sensing (km²)	Flood prone areas PGIIS (km²)	Overlap percentage
Dakar	10.34	101.42	10.19
Zinguinchor	91.91	2992.43	3.07
Diourbel	2.99	1 093.56	0.27
Saint-Louis	309.2	9 666.56	3.20
Tambacounda	59.21	9 739.77	0.61
Kaolack	18.31	1 476.10	1.24
Thies	14.15	1 313.32	1.08
Louga	41.14	6 031.24	0.68
Fatick	69.1	3 059.26	2.26
Kolda	18.17	2 578.36	0.70
Matam	77.41	9 449.34	0.82
Kaffrine	1.04	2 631.82	0.04
Kedougou	56.22	2 740.52	2.05
Sedhiou	10.53	1 662.70	0.63
Total	**779.54**	**54 536.34**	**1.43**

In terms of mapping, major differences emerge between the extents identified by GEE for August 2022 event and hydrological and hydraulic modeling, with spatial overlaps varying from one region to another. The analysis of these overlaps in the Dakar region is shown in Table 2, but with significant divergences. The total area provided by Google Earth Engine is approximately 18 times smaller than that provided by the 100-year hydrological and hydraulic model for the entire Senegal.

The Saint-Louis region, which was the most flooded during the 2022 event by GEE with an area of 309.02 km², now gives way, the Tambacounda region with an area of 9 739.77 km2 obtained by modelling (5th position in Google Earth flood mapping) and takes the second position (Table 2).

4.3. Exposed Population Assessment

Flood exposure was estimated using the intersection of flooded areas coming from Sentinel-1, GSW, HydroSHEDS and the GHLS population layer. We estimated that around 297 142 people (1.64 % of the Senegal total population) have been exposed around the contry. The results show that October is the greteast polupation exposure with 78 282 people (0.43 % about of the Senegal total population). Whilst the lower population exposure was estimated in September where 69 243 people (about 0.38 % of the Senegal total population) (Figure 5, Supplement Matarial 3). Total population exposure with the highest exposure in October do not correspond to the the month of the highest flooded areas August. Population exposure estimated using the GHLS dataset is greater in Dakar, Diourbel Thies and Saint-Louis regions with respectively about 100 707 people (about 2.58 % of the Dakar population), about 57 648 people (about 2.77 % of the Diourbel population), about 31 579 (about 1.27 of the population of Thies) and 26 581 (about 2.2 % of the population of Saint-Louis) (Figure 5, Supplement Matarial 3).

 doi:10.20944/preprints202404.1552.v1

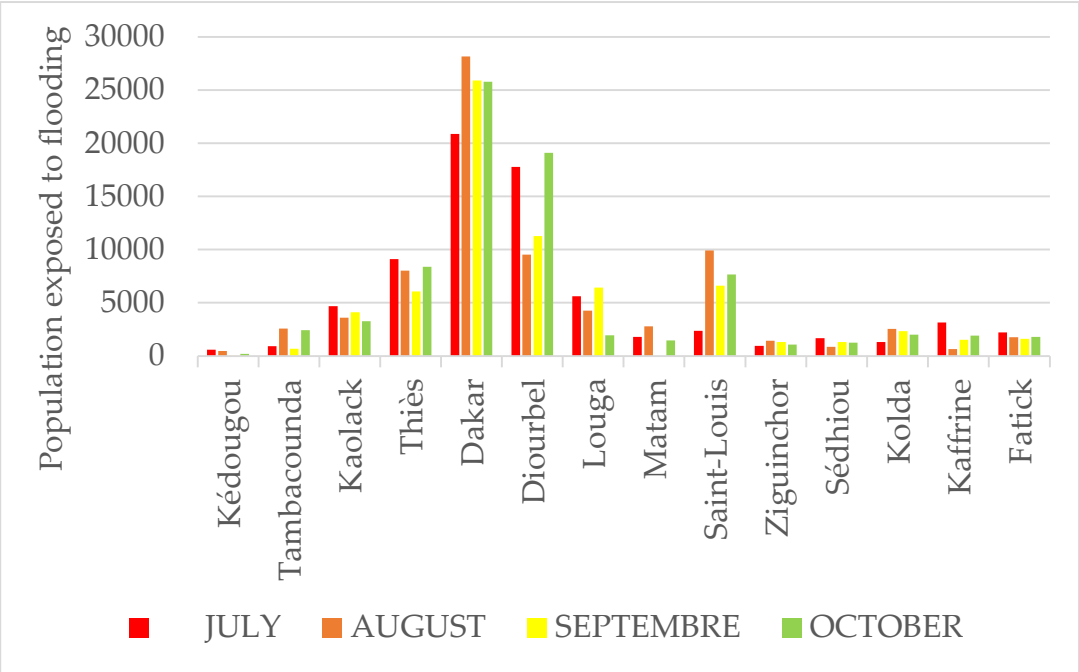

Figure 5. Population exposed to flooding from July to October of 2022 event estimated through intersection of GHLS population datasets with flooded areas in Google Earth Engine.

Figure 6 presents a spatial analysis of flood exposure in Dakar and Diourbel. In the Dakar region, the southeast area exhibits the highest concentration of people exposed to floods. Conversely, in the Diourbel region, the northwest and eastern parts demonstrate the highest exposure of people to floods.

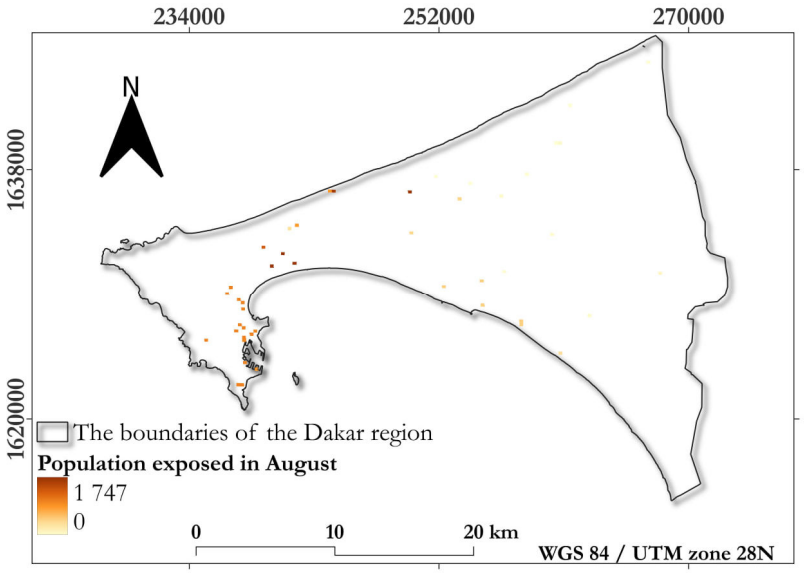

Preprints.org (www.preprints.org) | NOT PEER-REVIEWED | Posted: 25 April 2024 doi:10.20944/preprints202404.1552.v1

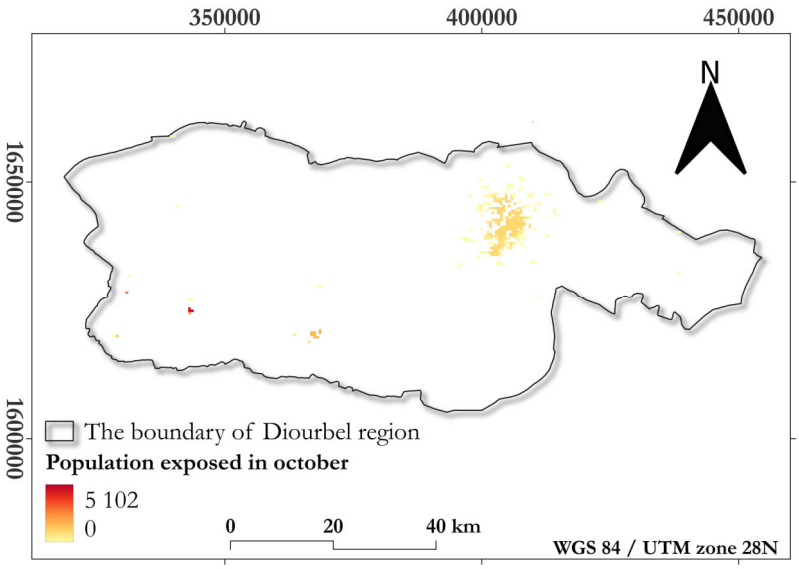

Figure 6. Spatial distribution of the two most population exposed regions to flooding through intersection of GHLS population datasets with flooded areas in Google Earth Engine. Yellow corresponds to low population density. While red highlights show densely populated areas. Legend numbers denote flood exposed people.

4.3. Exposed Urband and Cropland

Analysis of cropland and urban for the 2022 flood event showed that urban and farming areas represented respectively a total of 175 km² (7.12%) and 16 km² of farmland (1.05%). Dakar Diourbel and Ziguinchor have the highest urban areas exposed to flooding. While Thies and Saint-Louis have the highest farmland exposed to flooding (Figure 7, Supplement Matarial 4).

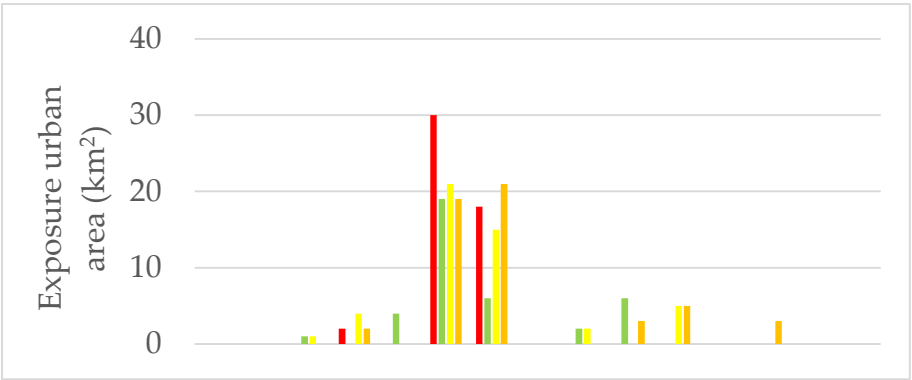

 doi:10.20944/preprints202404.1552.v1

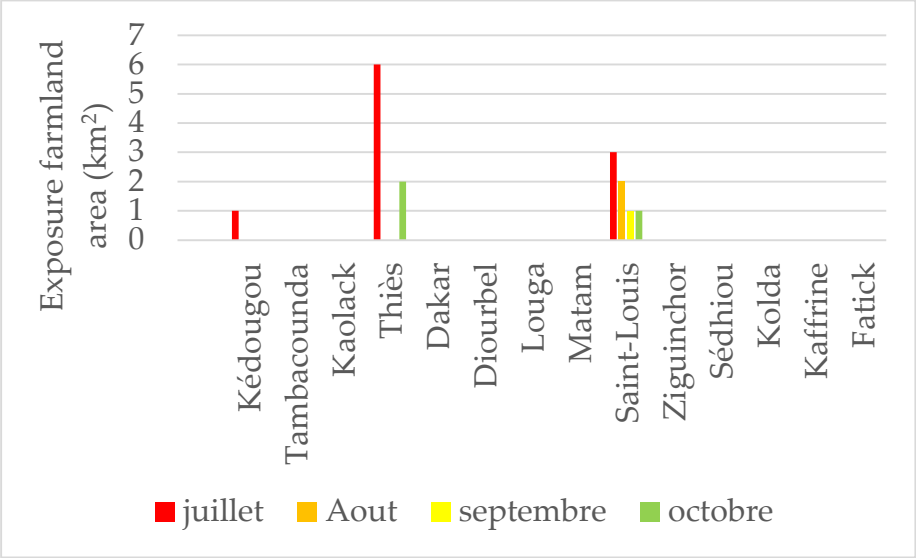

Figure 7. Urban and farmland exposed to flooding with intersection of Land cover MODIS datasets with flooded areas in Google Earth Engine.

5. Discussion

Mapping flooded areas and assessing exposure is particularly challenging in data-scarce regions like Senegal. Access to rapid, robust, and practical methodologies is crucial for flood mapping and subsequent mitigation efforts. In this study, we employed a spatial context approach within the Google Earth Engine (GEE) framework. Our objectives were twofold: firstly, to integrate satellite imagery, Global Surface Water data, and HydroSHEDS to delineate flooded areas for 2022 on a national scale, comparing them with hydrological modeling's centennial flood-prone areas. Secondly, we aimed to evaluate flood exposure concerning population density, urban areas, and farmland. By employing these methods, we have showcased the strengths and opportunities provided by the GEE platform for flood monitoring.

Robustness and reproducibility of our Google Earth Engine methodology for flood analysis.

The robustness and reproducibility of our flood analysis methodology using Google Earth Engine are evident. We have successfully demonstrated its capability to estimate flooded areas and assess exposure on a nationwide scale by leveraging freely available resources and a resilient web platform for cloud-based processing of Sentinel-1 data. A key advantage of utilizing this web-based platform is its computational speed, facilitated by outsourcing the processing workload to Google's powerful servers. Moreover, the platform provides access to a diverse range of continually updated datasets directly within the integrated code editor. This functionality expands the scope of flood monitoring, enabling potential near real-time flood mapping not only at the national level but also at continental or global scales, as evidenced by recent studies [11–42]. Crucially, this approach obviates the need to download raw imagery, enhancing efficiency.

Access to Google Earth Engine is freely available for academic and scientific research purposes but requires an activated Google account.

(https://earthengine.google.com/platform/).

The workflow implemented within the platform, combined with the simplicity of reproducibility through JavaScript—a user-friendly yet potent programming language for geospatial information analysis—ensures comprehensive documentation of all data and algorithms in an online repository. The shareable and publicly accessible GEE script, complete with linked data, can be rerun by any new flood analyst, ensuring the transparency and reproducibility of our results. This emphasis on reproducibility addresses a significant concern in many published studies [43], and also fosters collaboration and the advancement of flood hazard or management research in other regions of Africa or globally.

Accuracy and limitations of flooded areas mapping using sentinel-1 images.

 doi:10.20944/preprints202404.1552.v1

Our study showcases the potential of flood mapping using Sentinel-1 data, coupled with the integration of global flood datasets like GSW, to achieve higher accuracy in estimating flood areas compared to using optical satellite-based datasets. Optical images often yield lower accuracy in delineating flooding due to issues such as cloud cover and a coarse revisit time (16 days). In contrast, Sentinel-1 satellite data offers advantages in detecting flooded areas due to its radar transmission in the microwave spectrum, which remains unaffected by cloud cover, heavy rain, and low visibility, and can operate even at night [44,45]. However, it's worth noting that Sentinel-1 images may tend to underestimate flooded areas due to their spatial resolution (10 m), which may not be sufficient to capture all flooded areas [11] . Nonetheless, at the scale of our study, these images can provide a satisfactory view of flooded areas. For smaller-scale assessments, we recommend considering radar images with much higher spatial resolutions, such as TerraSAR-X datasets [46], covering at least one region, and comparing the results obtained with Sentinel-1 data. Despite Sentinel-1's revisit period of 6 days, it might still underestimate flooded areas. In such cases, frequent satellite observations become critical for exhaustive mapping of flooded areas.

Temporal analysis of flooding extents in all regions of Senegal during the July, August, September, and October 2022 event reveals that the Saint-Louis region experienced the most significant flooding. This can likely be attributed to the combination of overflowing floodwaters in the Senegal River (Saint-Louis), potentially triggered by heavy rains, urban runoff, and rising groundwater.

The highest flooded areas were observed in August 2022, a trend undoubtedly linked, in part, to the heavy rainfall recorded by the National Agency of Civil Aviation and Meteorology during this month. Total rainfall for August reached 105 mm, with an average daily rainfall of 3.36 mm, and a record single-day rainfall of 28.9 mm. Similar rainfall patterns were observed in the Saint-Louis region, contributing to the significant flooding. It's important to note that while there is a strong correlation between rainfall and flooding, various contributing factors such as infrastructure failures, pipeline blockages, overflow of lakes, and discharge of household septic tanks by the local population were discussed previously by Sy et al [12] in an earlier paper.

We observed lower agreement between flooded areas derived from this study using Sentinel-1 data and those derived from hydrological and hydraulic modeling conducted by PGIIS. This reduced agreement highlights both the strengths and limitations of satellite-based and modeling approaches. Notably, our results significantly deviate from the scenario corresponding to 100-year flood events in terms of flooded areas. However, by combining the strengths and the complementarity of Google Earth Engine (remote sensing observation over 4 months) and hydrological modeling (estimating occurrence for a 100-year return period), stakeholders can benefit from a more comprehensive understanding of flood risk. Remote sensing offers real-time spatial information, while hydrological modeling provides predictive capabilities and insights into the underlying processes driving flooding events. Together, these approaches enhance decision-making processes, risk assessment, and disaster management efforts aimed at mitigating the impacts of floods. In this study, emphasis should be placed on regions such as Dakar where the overlap between remote sensing and modeling is more significant for mitigation measures. Consequently, targeted mitigation measures and the allocation of adequate resources in such regions are crucial.

Insights and futures implications in flood exposure

The existing global databases of population distribution and density from GHLS datasets, combined with recently updated land cover data from Modis Global Land Cover, offer great potential for assessing national and spatially detailed exposure to flooding in terms of population, urban areas, and farmland in Senegal. Previous studies have shown that the increase in population exposure mainly results from flooded areas and population density datasets used [11–47] . In our study, Dakar and Diourbel are the most exposed regions, even though they do not have the most extensive flooded areas. This can be explained by the high population density in these regions compared to others [33]. Dakar, being the capital of Senegal, and Diourbel, the religious region of the largest brotherhood in the country, are the most densely populated regions.

 doi:10.20944/preprints202404.1552.v1

The population density in the GHLS datasets used in this work is based on the classification of building footprints from fine-scale satellite imagery, allowing for the distribution of the population over a smaller, more concentrated area. However, other databases such as WorldPop model a non-zero population density in almost the entire region, which means that the population is present in flooded areas. This may result in differences depending on the database used. Future work could improve estimates of the population exposed to flooding by further integrating national census data from the National Agency of Statistics and Demography [33]. The flood exposure results from this national census data as well as from other global databases can be compared with the results provided by GHLS datasets. Furthermore, we could improve flood-exposed population estimates by incorporating social media population data [48].

In terms of flood exposure, absolute numbers provide an indication of the magnitude of an issue but lack context regarding its severity relative to the population size. Relative figures enable comparison of exposure levels between different regions of Senegal, considering their respective population sizes. By considering relative figures, it becomes possible to identify the most exposed populations or regions proportionally to their size. Relative figures facilitate tracking changes in exposure over time, considering demographic growth or changes in population distribution. Considering both absolute and relative figures is crucial for a comprehensive assessment of the impact of a situation on a given population, leading to a better understanding of exposure reality and informed decision-making in risk management. That's why in this paper alongside absolute numbers, we present relative figures.

As mentioned by authors such as Rentschler et al [22], the results of flood-exposed populations cannot provide a complete picture alone. Here, it is crucial to also consider the income levels of flood-exposed populations by region, as these can serve as a proxy for people's ability to mitigate, withstand, cope with, and recover from floods. Similarly, flood-exposed populations in the Dakar region are more likely to have access to rapid government support systems in post-disaster situations compared to those in regions like Kédougou and Tambacounda. Floods in low-income areas are documented to have devastating and lasting impacts on livelihoods. Thus, actions aimed at strengthening disaster prevention and recovery capacity are most urgently needed where low income and flood exposure coincide.

The total population in Senegal is expected to increase in the future [33], regardless of the population or flood dataset used. The increase in population exposure will primarily result from increases in flood extent and demographics, so we can expect increases in population exposure in the future. In any case, we could compare the observations from this study with estimates in 2030 to identify regions in slowing, continuing, or increasing flood exposure trajectories. This analysis may enable prioritization of adaptation measures in regions where flood exposure has been growing or is expected to grow faster than the total population, especially under changing climate conditions.

The exposure of agricultural areas appears to be greatly underestimated by MODIS dataset. This underestimation could be due to their spatial resolution, but also to a classification that is not verified by field studies. It is possible that agricultural areas are classified into categories such as forests or others. Moreover, previous studies have shown that exposure estimated using this data is underestimated [11]. Therefore, it will be necessary in the future to find a method to verify this data, especially when working on a national scale.

6. Conclusions

This study has presented a robust framework, utilizing the GEE web platform, for mapping flood extent and exposure at a national scale in Senegal. Our results demonstrate the efficacy of combining radar satellite data with GWS and HydroSHEDS, enabling the rapid mapping of flood across expansive area of 196.722 km^2. Notably, our satellite imagery data align slightly with flood prone areas corresponding to the 100-year scenario. Furthermore, through the utilization of flood extent maps, we have successfully assessed flood exposure across the entire country. These results underscore the importance of prioritizing flood mitigation and adaptation measures in Senegal. The localized flood extent maps and flood exposure assessments generated by this study hold significant

potential for enhancing flood risk assessment and supporting the implementation of the Integrated Flood Management project. They provide valuable insights for informed decision-making and proactive disaster management strategies in Senegal.

Supplementary Materials: The following supporting information can be downloaded at: www.mdpi.com/.../...

Author Contributions: B.S. and FB.B. conceived the original ideas. B.S FBB and HD drafted the original manuscript. B.S. and F.BB. carried out data processing. B.S. and H.D. revised the original manuscript. All authors have read and agreed to the published version of the manuscript.

Data Availability Statement: The majority of the data is available on the Google Earth Engine platform. The centennial modeling data was provided to us by submitting a request to PGIIS. For more information, please contact us.

Acknowledgments: The authors would also like to thank Mr. Diadji Cisse, Mr. Hamidou Konate, and Mr. Martin Bortolotti for providing them with the data from the PGIIS project.

Conflicts of Interest: The authors declare no conflicts of interest.

References

1. Ndehedehe, C. Hydro-Climatic Extremes: Climate change and human influence. In *Hydro-Climatic Extremes in the Anthropocene*; Springer International Publishing, **2023**; pp 25–55. https://doi.org/10.1007/978-3-031-37727-3_2.
2. UNISDR-CRED. The Human cost of weather-related disasters 1995–2015–, The United Nations office for Disaster Risk Reduction (UNISDR) and Centre for Research on the Epidemiology of Disasters (CRED), 1-30, 2015.
3. EM-DAT. The OFDA/CRED International Disaster Database, at: https://public.emdat.be/data, last access: 24 January 2024.
4. Chen, Y.; Zhou, H.; Zhang, H.; Du, G.; Zhou, J. Urban flood risk warning under rapid urbanization. *Environ. Res.* **2015**, *139*, 3–10. https://doi.org/10.1016/j.envres.2015.02.028.
5. Sy, B.; Frischknecht, C.; Dao, H.; Consuegra, D.; Giuliani, G. Reconstituting past flood events: the contribution of citizen science. *Hydrol. Earth Syst. Sci.* **2020**, *24* (1), 61–74. https://doi.org/10.5194/hess-24-61-2020, 2020.
6. de Moel, H.; Aerts, J. C.; Koomen, E. Development of flood exposure in the Netherlands during the 20th and 21st Century. *Global. Environmental. Change* **2011**, *21* (2), 620–627. https://doi.org/10.1016/j.gloenvcha.2010.12.005.
7. Rahman, M.; Ningsheng, C.; Mahmud, G. I.; Islam, M. M.; Pourghasemi, H. R.; Ahmad, H.; Habumugisha, J. M.; Washakh, R. M. A.; Alam, M.; Liu, E. Flooding and its relationship with land cover change, population growth, and road density. *Geoscience Frontiers.* **2021**, *12* (6), 101224. https://doi.org/10.1016/j.gsf.2021.101224
8. Hirabayashi, Y.; Mahendran, R.; Koirala, S.; Konoshima, L.; Yamazaki, D.; Watanabe, S.; Kim, H.; Kanae, S. Global Flood Risk under Climate Change. *Nature. Climate. Change* **2013**, *3* (9), 816–821. https://doi.org/10.1038/nclimate1911.
9. Kedowide, C.M.G ; Cissé, O. Adaptating to flooding impact in Yeumbeul Nord, a suburb of Dakar, Senegal: Generation of knowledge and of Mapping Data at the crossroads of a need for the territorialization of spatialized phenomena, in proceedings of the resilient cities, Bonn, Germany, 29-31 May. **2014**. 1-20, available at http://hdl.handle.net/10625/53299, last access 08 March 2024.
10. Waca. Floods in Senegal, are retention basins part of the Solution? at: https://www.wacaprogram.org/article/floods-senegal-are-retention-basins-part-solution, last access: 8 March 2023.
11. Li, C.; Dash, J.; Asamoah, M.; Sheffield, J.; Dzodzomenyo, M.; Gebrechorkos, S. H.; Anghileri, D.; Wright, J. Increased flooded area and exposure in the white Volta river basin in Western Africa, identified from multi-Source remote sensing data. *Scientific. Reports.* **2022**, *12* (1), 3701. https://doi.org/10.1038/s41598-022-07720-4
12. Sy, B. Approche multidisciplinaire de l'évaluation de l'aléa d'inondation à Yeumbeul Nord, Dakar, Sénégal: La contribution de La science citoyenne, thèse Université de Genève.**2019**. https://doi.org/10.13097/archive-ouverte/unige:126388.
13. Muis, S.; Güneralp, B.; Jongman, B.; Aerts, J. C.; Ward, P. J. Flood Risk and Adaptation Strategies under Climate Change and Urban Expansion: A Probabilistic Analysis Using Global Data. *Science of the Total Environment.* **2015**, *538*, 445–457. https://doi.org/10.1016/j.scitotenv.2015.08.068.
14. DeVries, B.; Huang, C.; Armston, J.; Huang, W.; Jones, J. W.; Lang, M. W. Rapid and robust monitoring of flood events using Sentinel-1 and Landsat data on the Google Earth Engine. *Remote Sensing of Environment.* **2020**, *240*, 111664. https://doi.org/10.1016/j.rse.2020.111664.

15. Ward, D. P.; Petty, A.; Setterfield, S. A.; Douglas, M. M.; Ferdinands, K.; Hamilton, S. K.; Phinn, S. Floodplain inundation and vegetation dynamics in the Alligator rivers region (Kakadu) of Northern Australia assessed uing optical and radar remote sensing. *Remote Sensing of Environment.* **2014**, *147*, 43–55. https://doi.org/10.1016/j.rse.2014.02.009
16. Singha, M.; Dong, J.; Sarmah, S.; You, N.; Zhou, Y.; Zhang, G.; Doughty, R.; Xiao, X. Identifying floods and flood-affected paddy rice fields in Bangladesh based on Sentinel-1 imagery and Google Earth Engine. *ISPRS J. Photogrammetry and Remote Sensing.* **2020**, *166*, 278–293. https://doi.org/10.1016/j.isprsjprs.2020.06.011.
17. Gorelick, N.; Hancher, M.; Dixon, M.; Ilyushchenko, S.; Thau, D.; Moore, R. Google Earth Engine: planetary-scale geospatial analysis for everyone. *Remote sensing of Environment.* **2017**, *202*, 18–27. https://doi.org/10.1016/j.rse.2017.06.031.
18. Tiwari, V.; Kumar, V.; Matin, M. A.; Thapa, A.; Ellenburg, W. L.; Gupta, N.; Thapa, S. Flood inundation mapping-Kerala 2018; Harnessing the Power of SAR, Automatic threshold detection method and Google Earth Engine. *PLoS One* **2020**, *15* (8), e0237324. https://doi.org/10.1371/journal.pone.0237324.
19. Moharrami, M.; Javanbakht, M.; Attarchi, S. Automatic Flood Detection Using Sentinel-1 Images on the Google Earth Engine. *Environmental monitoring and assessment.* **2021**, *193*, 1–17. https://doi.org/10.1007/s10661-021-09037-7.
20. Johary, R.; Révillion, C.; Catry, T.; Alexandre, C.; Mouquet, P.; Rakotoniaina, S.; Pennober, G.; Rakotondraompiana, S. Detection of large-scale floods using Google Earth Engine and Google Colab. *Remote Sensing.* **2023**, *15* (22), 5368. https://doi.org/10.3390/rs15225368.
21. Ghouri, A. Y.; Khan, A.; Raoof, H.; Miandad, M.; Rehman, G. Flood mapping using the Sentinel-1 SAR dataset and application of the change detection approach technique (CDAT) to the Google Earth Engine in Sindh Province, Pakistan. *Ecological Questions.* **2024**, *35* (2), 1–18. https://doi.org/ 10.12775/EQ.2024.024.
22. Rentschler, J.; Salhab, M.; Jafino, B. A. Flood exposure and poverty in 188 countries. *Nature Communication.* **2022**, *13* (1), 3527. https://doi.org/10.1038/s41467-022-30727-4
23. Van Den Homberg, M.; Susha, I. Characterizing data ecosystems to support official statistics with open mapping data for reporting on sustainable development Goals. *ISPRS International Journal of Geo-Information.* **2018**, *7* (12), 456. https://doi.org/10.3390/ijgi7120456
24. Wouters, L.; Couasnon, A.; De Ruiter, M. C.; Van Den Homberg, M. J.; Teklesadik, A.; De Moel, H. Improving flood damage assessments in data-scarce areas by retrieval of building characteristics through UAV image segmentation and machine learning–a case study of the 2019 floods in Southern Malawi. *Natural Hazards and Earth System Sciences.* **2021**, *21* (10), 3199–3218. https://doi.org/10.5194/nhess-21-3199-2021
25. Cea, L.; Álvarez, M.; Puertas, J. Estimation of flood-exposed population in data-scarce regions combining satellite imagery and high resolution hydrological-hydraulic modelling: a case study in the Licungo Basin (Mozambique). *Journal of Hydrology: Regional Studies.* **2022**, *44*, 101247. https://doi.org/10.1016/j.ejrh.2022.101247.
26. Mbow, C.; Diop, A.; Diaw, A.; Niang, C. I. Urban sprawl development and flooding at Yeumbeul suburb (Dakar-Senegal). *African Journal of Environmental Science and Technology.* **2008**, *2* (4), 075–088.
27. Sy, B.; Frischknecht, C.; Dao, H.; Giuliani, G.; Consuegra, D.; Wade, S.; Kêdowidé, C. Participatory approach for flood risk assessment: the case of Yeumbeul Nord (YN), Dakar, Senegal. *WIT Transactions on the Built Environment*. **2016**, *165*, 331–342. https://doi.org/10.2495/UW160291, 2016.
28. PGIIS: Cartographie du risque d'inondation à l'échelle nationale; *Projet de Gestions Intégrée des Inondations au Sénégal (PGIIS)*. **2022**; 1–126.
29. WHO: State of the Climate in Africa 2022. *Word Meteorological Organization*. **2022**; 1330; 2023; 1-30, at https://www.google.com/url?sa=t&rct=j&q=&esrc=s&source=web&cd=&ved=2ahUKEwjJsIaPieWEAxU89LsIHZ3eBdAQFnoECA4QAQ&url=https%3A%2F%2Flibrary.wmo.int%2Fviewer%2F67761%2Fdownload%3Ffile%3D1330_State-of-the-Climate-in-Africa-2022_en.pdf%26type%3Dpdf%26navigator%3D1&usg=AOvVaw1N9WC_I_8xrPc-x4fs7z2i&opi=89978449, last access 08 March 2024.
30. UNICEF: Responds to the Immediate Needs of Flood-Affected Children and Families in Senegal, at https://www.unicef.org/senegal/en/stories/unicef-responds-immediate-needs-flood-affected-children-and-families-senegal, last access 08 March 2024.
31. OCHA: West and Central Africa: Flooding Situation - As of 16 August 2022., at https://reliefweb.int/report/congo/west-and-central-africa-flooding-situation-16-august-2022**,** last access 08 March 2024.
32. ANAT: Atlas Cartographique; *Agence Nationale de l'Aménagement du Territoire*: Dakar, **2020**; 1–69.
33. ANSD: 5ème Recencement Général de La Population et de l'habitat; *Agence Nationale de la Statistique et de la Démographie*, 2023; 1–21.
34. ANSD: Situation Économique et Sociale régionale; *Agence Nationale de la Statistique et de la Démographie*, 2013; 1-129.

35. Torres, R.; Snoeij, P.; Geudtner, D.; Bibby, D.; Davidson, M.; Attema, E.; Potin, P.; Rommen, B.; Floury, N.; Brown, M. GMES Sentinel-1 Mission. *Remote sensing of environment.* **2012**, *120*, 9–24. https://doi.org/10.1016/j.rse.2011.05.028
36. Malenovský, Z.; Rott, H.; Cihlar, J.; Schaepman, M. E.; García-Santos, G.; Fernandes, R.; Berger, M. Sentinels for Science: Potential of Sentinel-1,-2, and-3 missions for scientific observations of ocean, cryosphere, and land. *Remote Sensing of environment.* **2012**, *120*, 91–101. Malenovský, Z., Rott, H., Cihlar, J., Schaepman, M. E., García-Santos, G., Fernandes, R., & Berger, M. (2012). Sentinels for science: Potential of Sentinel-1,-2, and-3 missions for scientific observations of ocean, cryosphere, and land. *Remote Sensing of environment*, *120*, 91-101. https://doi.org/10.1016/j.rse.2011.09.026. https://doi.org/10.1016/j.rse.2011.09.026
37. Twele, A.; Cao, W.; Plank, S.; Martinis, S. Sentinel-1-Based Flood Mapping: A fully automated processing Chain. *International Journal of Remote Sensing.* **2016**, *37* (13), 2990–3004. Twele, A., Cao, W., Plank, S., & Martinis, S. (2016). Sentinel-1-based flood mapping: a fully automated processing chain. *International Journal of Remote Sensing*, *37*(13), 2990-3004. https://doi.org/10.1080/01431161.2016.1192304
38. Clement, M. A.; Kilsby, C.; Moore, P. Multi-temporal synthetic aperture radar flood mapping using change detection. *Journal of Flood Risk Management.* **2018**, *11* (2), 152–168. https://doi.org/10.1111/jfr3.12303.
39. ESA. Revisit and coverage frequency of the Sentinel-1 constellation, showing which areas are mainly covered with descending or ascending imagery, at Https://Sentinel.Esa.Int/Web/Sentinel/Copernicus/Sentinel-1/Acquisition-Plans, last access: 24 January 2024.
40. Cian, F.; Marconcini, M.; Ceccato, P. Normalized Difference Flood Index for Rapid Flood Mapping: Taking Advantage of EO Big Data. *Remote Sensing of Environment.* **2018**, *209*, 712–730. https://doi.org/10.1016/j.rse.2018.03.006.
41. European Commission Global Human Settlement Layer - Open and free data and tools for assessing the human presence on the planet, available at: https://human-settlement.emergency.copernicus.eu/p2023Release.php, last access 22 April 2024.
42. Tellman, B.; Sullivan, J. A.; Kuhn, C.; Kettner, A. J.; Doyle, C. S.; Brakenridge, G. R.; Erickson, T. A.; Slayback, D. A. Satellite imaging reveals increased proportion of population exposed to floods. *Nature*. **2021**, *596* (7870), 80–86. https://doi.org/10.1038/s41586-021-03695-w.
43. Kar, B.; Schumann, G. Reproducibility and replicability of flood models. *Hydrological processes*. **2022**. 36(9), e14666. https://doi.org/10.1002/hyp.14666
44. Amitrano, D.; Di Martino, G.; Iodice, A.; Riccio, D.; Ruello, G. Unsupervised rapid flood mapping using Sentinel-1 GRD SAR images. *IEEE Transactions on Geoscience and Remote Sensing.* **2018**, *56* (6), 3290–3299. https://doi.org/ 10.1109/TGRS.2018.2797536
45. Nghia, B. P. Q.; Pal, I.; Chollacoop, N.; Mukhopadhyay, A. Applying Google Earth Engine for flood mapping and monitoring in the downstream Provinces of Mekong River. *Progress in Disaster Science.* **2022**, *14*, 100235. https://doi.og/10.1016/j.pdisas.2022.100235
46. Giustarini, L.; Hostache, R.; Matgen, P.; Schumann, G. J.-P.; Bates, P. D.; Mason, D. C. A Change detection approach to flood mapping in urban areas using TerraSAR-X. *IEEE Transactions on Geoscience and Remote Sensing.* **2012**, *51* (4), 2417–2430. https://www.scopus.com/record/display.uri?eid=2-s2.0-84875707692&origin=inward&txGid=80f7a1beeeb5efc7c78e7e46e6626b75
47. Smith, A.; Bates, P. D.; Wing, O.; Sampson, C.; Quinn, N.; Neal, J. New estimates of flood exposure in developing countries using high-resolution population data. *Nature Communication.* **2019**, *10* (1), 1814. https://doi.org/10.1038/s41467-019-09282-y
48. de Bruijn, J. A.; de Moel, H.; Jongman, B.; de Ruiter, M. C.; Wagemaker, J.; Aerts, J. C. A global database of historic and real-time flood events based on social media. *Scientific data* **2019**, *6* (1), 311. https://doi.org/10.1038/s41597-019-0326-9